Journal of Applied Polymer Science

Investigations on Clay Dispersion in Polypropylene/Clay Nanocomposites Using Rheological and Microscopic Analysis

Saikat Banerjee,[1] Mangala Joshi,[2] Anup K. Ghosh[1]

[1]Centre for Polymer Science and Engineering, Indian Institute of Technology Delhi, New Delhi 110016, India
[2]Department of Textile Technology, Indian Institute of Technology Delhi, New Delhi 110016, India
Correspondence to: A. K. Ghosh (E-mail: anupkghosh@gmail.com)

ABSTRACT: Morphology assessment plays an important role as the ultimate properties of the processed nanocomposites mainly depend upon the morphology. This study focuses on the evaluation of polypropylene/clay nanocomposite structure using rheological and transmission electron microscopic investigation. Melt processing of nanocomposite was carried out on a co-rotating twin screw extruder. Maleic anhydride grafted polypropylene (PP-*g*-MA) was used as a compatibilizer to facilitate better mixing of clay in polypropylene. The effect of compatibilizer to clay ratio on dispersion was analyzed through rheological data. An increase in complex viscosity and storage modulus with increase in compatibilizer content is observed at lower frequency region. Shifting of crossover frequencies to a lower value also indicate better exfoliation. Improved exfoliated morphology was also corroborated by Cole–Cole and inverse loss tangent plots. Transmission electron microscopy (TEM) micrograph based unique statistical image analysis was carried out using ImageJ software. A compatibilizer to clay content of 2 : 1 was found to be the optimum composition which was further supported by dielectric and mechanical properties. © 2013 Wiley Periodicals, Inc. J. Appl. Polym. Sci. 130: 4464–4473, 2013

KEYWORDS: morphology; rheology; dielectric properties

Received 3 March 2013; accepted 23 May 2013; Published online 24 July 2013
DOI: 10.1002/app.39590

INTRODUCTION

Processing of polymer/clay nanocomposites by melt extrusion generally leads to a morphology comprised of exfoliated and/or intercalated clay platelets along with tactoids stacks.[1–5] The extent of exfoliation and intercalation depends upon factors such as applied shear, diffusion of polymer chains into clay gallery, and surface morphology of the clay layers.[6] The induced shear stress applied upon clay tactoids by the polymer melt becomes effective in breaking down the tactoids which thus increases the distance between individual clay stacks. Diffusion of polymer chains into the clay gallery plays an important role for dispersion of clay platelet into polymer matrix. Polymers are generally hydrophobic in nature whereas clays are known to be hydrophilic. Therefore, compatibility between polymer matrix and silicate layer surface of the clay is very crucial during melt processing of polymer/clay nanocomposites. In order to improve the affinity between the hydrophilic clay surface and the hydrophobic polymer chains, maleic anhydride grafted polypropylene (PP-*g*-MA) is used as compatibilizer.[7,8] Higher content of compatibilizer is detrimental towards mechanical properties, whereas low content is insufficient for better dispersion and exfoliation. Moreover, higher percentage of maleic anhydride grafting reduces the chain length and average molecular weight of the PP molecules in PP-*g*-MA which results in inferior mechanical properties. Therefore, an optimum grafting is preferable. Melt rheology is found to be an important tool to assess state of dispersion of filler in polymer and to understand the structure–property relationship in polymer/clay nanocomposites.[9–11] The intercalated and exfoliated morphology can be interpreted by considering shear thinning behavior and the flow curve trend of the processed nanocomposites.[12] The use of rheological technique enables microstructure evaluation. It has been extensively used in the study of nanocomposites in conjunction with basic characterization techniques like X-ray diffraction, mechanical, and transmission electron microscopy. The advantage of rheology is that the measurements can be performed in the molten state to study the response of the nanocomposites to both linear and non-linear deformation. The useful information that can be derived from dynamic rheology are storage modulus (G'), loss modulus (G''), damping behavior ($\tan \delta$) and complex viscosity (η^*). These experiments give the idea about elastic and viscous response as well as zero shear viscosity, and relaxation behavior of the materials. These parameters are dependent on molecular structure of the material and sensitive to size, shape, and morphology of the fillers in polymer matrix. Incorporation of nanofillers in polymer matrix induces an alteration in molecular mobility and crystallinity of

Table I. Screw Profile for the Twin Screw Extruder

Barrel zone	Feed	Die
Screw configuration	8 FS + KB 30/7 + KB 60/5 + KB 90/6 + 5 FS + KB 60/8 + KB 90/8 + 2 FS + Ext	

FS: Forwarding screw elements, L = D. KB 30/7: Kneading blocks with 30°stagger angle, 7 kneading discs per block, L = 0.25 D. Ext: Extrusion screw, L = 1.5 D.

the matrix. Polymer nanocomposites seem to exhibit pronounced elastic properties as well as delayed relaxation time as compared to the neat resin.

X-ray diffraction technique is another important tool to evaluate the morphology along with transmission electron microscopy (TEM). But, in some cases, it can mislead to distinguish an exfoliated structure from agglomerated one. TEM also needs advancement as it probes only a specific region of the sample and may not be representative of the whole sample. Therefore, a statistical image analysis technique[13] was used to measure the thickness, length, aspect ratio, and inter-particle distance of the dispersed nanoclays in the polymer resin to assess the dependence of morphology on compatibilizer to organo-clay ratio. Information about the various particle parameters like tactoid percentage, tactoid length, and aspect ratio was extracted from this study. Dielectric and mechanical tests were performed in support for these analyses. When a polymer with dielectric property either in solid or in melt form is subjected to an external electrical field, the dipoles are oriented in the field direction.[14] This phenomenon can be described by the complex relative permittivity ε^* as,

$$\varepsilon^* = \varepsilon' - i\varepsilon'' \quad (1)$$

In eq. (1), the real part, dielectric permittivity ε' is associated with the polarization or capacitance of the material and the imaginary part ε'', the dielectric loss, is related to the conductance. The dielectric constant may be defined as the ratio of the capacitance of electrode couple with the dielectric material sandwiched between them to the capacitance of the same electrodes in presence of vacuum. The dielectric constant of vacuum is considered as unity. For polar polymers, at very low alternating current frequencies the dipoles have enough time to align in the field direction and dielectric constant is high. But, at very high frequencies, the dipoles of the polymer molecules do not have sufficient time to align before the field direction changes and hence the dielectric constant remains lower.[15] In the case of polymer/clay nanocomposites, as the clay starts to disperse and exfoliate in the matrix, it creates a hindrance towards orientation of the polar matrix in presence of applied electric field and a drop in dielectric constant value is the evidence for this phenomenon.

In this study, melt rheological measurements were carried out to assess the clay dispersion in presence of compatibilizer. The effect of clay dispersion on solid-like behavior was predicted from loss tangent and Cole–Cole plot. The steady torque and apparent viscosity values estimated from mass flow rate during mixing in twin screw extruder are qualitative indicators of stress that is imposed by the molten polymer on fillers. A TEM-based quantitative statistical image analysis technique was used to measure the dispersion.

EXPERIMENTAL

Materials and Methods

The isotactic polypropylene (iPP, REPOL H110 MA, MFI∼11) used in this study was procured from Reliance Industries, India. Maleic anhydride-grafted polypropylene (PP-*g*-MA, OPTIM P-406) with a melt index of 24 g/10 min at 190°C and 2.16 kg load was procured from Pluss Polymer India. The clay, Cloisite 15A, was procured from Southern Clay Products, USA, which has a cation exchange capacity of 125 meq/100 g, and was modified with dimethyl, hydrogenated tallow, and quaternary ammonium salts.

The melt mixing was done in a Prism Eurolab-16 co-rotating twin screw extruder having a high shear screw configuration for better mixing (Table I).[16] The temperature profile (160–200°C) was selected such as to minimize the degradation of the polymer during processing. Before melt processing, all the components were dried at 80°C for 24 h. The feed rate (25% of the maximum) and screw speed at 300 rpm was kept constant. The optimized concentration of clay chosen for all the experiments was 4 phr (Table II).

Characterization *T*echniques

The dynamic rheological measurements were carried out on Bohlin C-VOR rotational rheometer (Malvern Instruments, UK). Parallel plate geometry with 25 mm diameter and 1 mm gap was used in all the tests. All the samples were initially tested using an amplitude sweep between 0.0001 to 10 strain units to determine the linear viscoelastic region (LVR). The frequency sweeps between 0.01–100 Hz at 0.1 strain unit were performed maintaining temperature at 200°C.

Table II. Formulations for the PP/Clay Nanocomposites Processed in Twin-Screw Extruder Varying Compatibilizer to Clay Ratio (MFI of PP = 11, Screw Speed = 300 rpm)

	PP/PP-*g*-MA/Clay (phr)			
Composition	100/0/4	100/4/4	100/8/4	100/12/4
Designation	NC/MA0*	NC/MA-C-1	NC/MA-C-2	NC/MA-C-3
Compatibilizer to clay ratio	-	1 : 1	2 : 1	3 : 1

*Without compatibilizer.

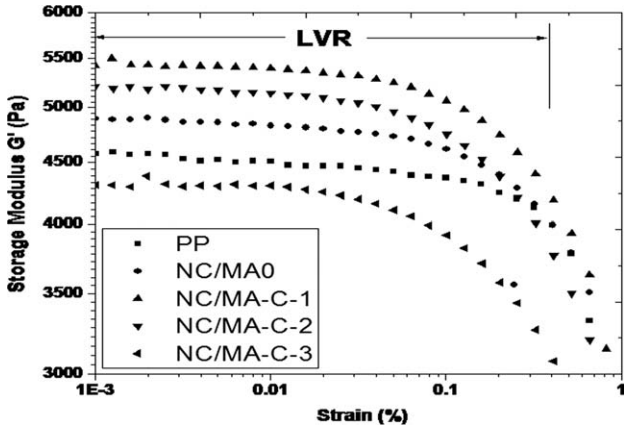

Figure 1. Linear viscoelastic region (LVR) of neat PP and PP/clay nanocomposites based on storage modulus.

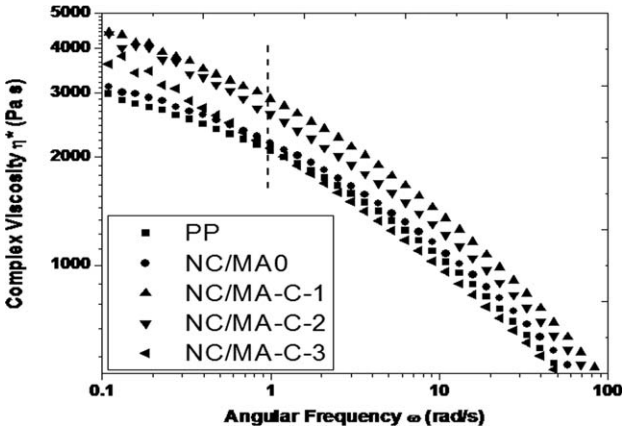

Figure 2. Complex viscosity as a function of frequency for neat PP and PP/clay nanocomposites.

For transmission electron microscopy (TEM) freshly cut glass knives with cutting edge of 45° were used to get the cryosections of 50 nm thickness by using a Leica Ultracut UCT microtome. JEOL-2100 electron microscope (Tokyo, Japan) having LaB6 filament and operating at an accelerating voltage of 200 kV was utilized to obtain the bright field images of the cryo-microtomed samples.

Dielectric parameters, such as capacitance was measured by a Hewlett-Packard 4192A LF Impedance Analyzer at various frequencies (10–10^6 Hz) at room temperature (30°C). Dielectric constants (ε) of the specimens were calculated using the relation,

$$C = \varepsilon\,\varepsilon_0(A/d) \quad (2)$$

where ε_0 is vacuum permittivity having the value of 8.85×10^{-12} F/m. C is the capacitance, A is the electrode area, and d is the thickness of the specimen. The samples were in circular film shape having a thickness of ~35 μm and coated with silver.

Tensile tests were performed at room temperature according to ASTM D638, using Zwick Z010 at a cross-head speed of 50 mm/min. Flexural tests were also done according to ASTM D790 using the same instrument. Reported mechanical data was the average of five tests on the same specimens.

RESULTS AND DISCUSSION

Rheological Studies

Linear viscoelastic region (LVR) determination is the preliminary requirement before commencing tests for frequency sweep to ensure that the micro-structure of the sample would not be perturbed by shear application. A strain sweep dynamic test was performed in order to characterize strain dependence viscoelastic response. The sample was subjected to increasing oscillatory strain amplitude at a particular frequency. In the linear region, the imposed deformation is not high enough to disturb the microstructure. On increasing the strain amplitude, the micro-structure commenced to respond by aligning in the flow direction and beyond a critical strain value the storage as well as loss modulus seemed to decrease. Figure 1 shows amplitude sweep results for polypropylene/clay nanocomposites performed at 200°C and 1 Hz frequency as a function of compatibilizer PP-*g*-MA to clay ratio at clay loading of 4 phr. At low strain, storage modulus follows a linear regime and after strain amplitude of 0.1% it shows a non-linearity. This transition point from linear viscoelastic to non-linear viscoelastic region is known as critical strain amplitude (γ_c). Depending upon the compatibilizer content at a particular clay loading and clay dispersion, this critical strain amplitude may shift. In case of unfilled polypropylene, the absence of nanoclay leads to retain its original micro-structure which is reflected by a wide linear viscoelastic region. It was observed that the modulus in LVR increased with addition of clay. Further increase was observed with addition of compatibilizer up to a compatibilizer to clay ratio of 2 : 1, however, the values decreased for the samples processed with compatibilizer to clay ratio of 3 : 1. An increase in compatibilizer content helps in clay dispersion that is reflected with an increase in modulus value. But use of higher compatibilizer (PP-*g*-MA) content beyond compatibilizer to clay ratio of 2 : 1 disturbs the polypropylene matrix crystallization resulting in a modulus value decrement.

Table II provides the formulations used in this study. Figure 2 represents the complex viscosity as a function of frequency for PP/PP-*g*-MA/organoclay nanocomposites at 200°C.[17] Addition of clay and compatibilizer lead to significantly higher viscosities and an earlier onset of shear thinning as compared to that of the unfilled polymer matrix at low frequency (below 1 rad/s). The strong interaction between dispersed clay layers and polymer chains with increase in compatibilizer content results in percolated network-like formation which resists flow. Higher viscosity ratios of nanocomposites as compared to neat polymer corroborate this fact (Table III). This non-Newtonian behavior at low frequencies for nanocomposites indicates the transformation from liquid-like to solid-like behavior.[18]

Frequency dependence viscoelastic behavior was studied at a strain of 0.01% in the linear viscoelastic region to study the microstructural change in the nanocomposite with an increase in compatibilizer to clay ratio. Figure 3(a) shows the frequency dependence of storage modulus (G') of neat PP, clay filled PP without compatibilizer and with compatibilizer having various compatibilizer to clay ratio obtained from the frequency sweep

Table III. Complex Viscosity, Viscosity Ratio, Crossover Frequency and Relaxation Time as a Function of Compatibilizer to Clay Ratio

Compositions	Complex viscosity at 0.1 rad/s (Pa s)	Complex viscosity ratio at 0.1 rad/s	Crossover frequency (Hz)	Relaxation time (s)
PP	2237	1.00	13.20	0.08
NC/MA0	2365	1.06	10.96	0.09
NC/MA-C-1	2899	1.29	9.12	0.11
NC/MA-C-2	3138	1.40	9.01	0.11
NC/MA-C-3	2342	1.05	7.59	0.13

test.[19,20] Increase in compatibilizer to clay ratio causes a systematic increase in G', especially at low frequency region (below 1 Hz), where G' becomes less frequency-dependent. At the higher compatibilizer to clay ratio, G' approaches a low frequency plateau, which means that the sample relaxes very slowly at long time scales. It has been reported that such solid-like viscoelastic behavior results from the formation of dense percolated network of platelets in polymer/clay nanocomposites.[21–24] At the higher content of compatibilizer (2 : 1) better exfoliation of the clay is observed which may be due to the formation of percolated network structure. At a frequency of ~0.01 Hz, the storage modulus G' for PP and clay filled PP without compatibilizer are observed to be 61.1 and 68.1 Pa, respectively, whereas compatibilized composite shows a modulus of 134 Pa and above. It implies that at 4 phr organo-clay content in the absence of compatibilizer (PP-*g*-MA), polymer–filler interaction is poor and thus leads to formation of macro-composite. At low frequency region, all the samples show a liquid like behavior ($G' < G''$) which is followed by a solid like behavior ($G' > G''$) beyond the crossover frequency (ω_x) [Figure 3(b)] where G'' implies to loss modulus. Considering Maxwell model, relaxation time (λ, in s) can be correlated with crossover frequency using the relation:

$$\tan\ \delta = 1/\omega\lambda, \tag{3}$$

where tan δ is the tangent of phase angle δ between G' and G'', ω is the angular frequency of oscillation. At crossover, tan $\delta = 1$ which implies $\lambda = 1/\omega_x$ i.e., relaxation time is inversely proportional to crossover frequency. The crossover frequency and relaxation time as a function of compatibilizer to clay ratio is shown in Table III. The shifting of crossover frequency towards lower side with addition of compatibilizer signifies development of pseudo-solid like behavior. The delay in relaxation time as observed in these samples is expected due to formation of network like structure of clay in presence of compatibilizer which acts as hindrance to the relaxation to polymer chains.

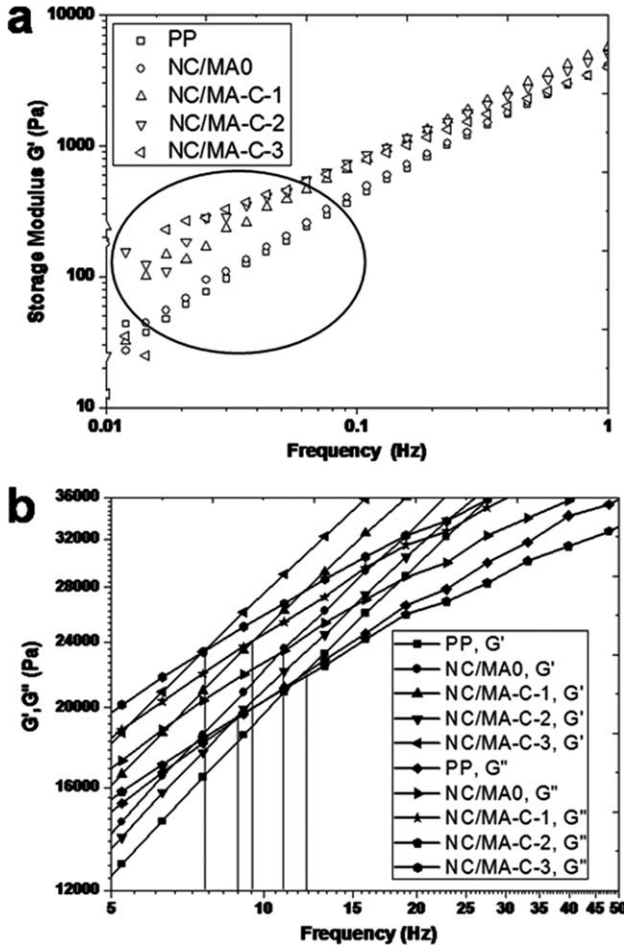

Figure 3. Frequency dependence of (a) storage modulus (G'), and (b) crossover frequency of neat PP and PP/clay nanocomposites.

In case of polymer nanocomposites, the first normal stress difference has two origins: the polymer matrix and the clay platelets. At low frequency, the clay platelets are not well oriented and held together to form a network-like structure which helps to create additional normal force compared to unfilled polymer resin. Thus, a part of normal force is related to the percolated network formation ability of the clay; whereas the other part is related to the polymer chain to sustain their coiled structure. Increase in compatibilizer content helps in exfoliation and consequently contributes to rise in normal stress [Figure 4(a)]. But, at higher frequency, the polymer chains orient in the flow direction along with clay platelets. Hence, less relaxation time is required to return to their original coil shape and consequently less normal force is created. The effect of clay morphology on solid-like behavior can be predicted considering stress relaxation measurement using Schwarzl method[25] [eq. (4)]. The stress relaxation modulus $G(t)$ can be estimated from dynamic moduli $G'(\omega)$ and $G''(\omega)$.[26]

$$G(t) = G'(\omega) - 0.56G''(\omega/2) + 0.2G''(\omega) \tag{4}$$

where $t = 1/\omega$. Figure 4(b) shows time dependency of stress relaxation modulus $G(t)$. A decrease in slope with time

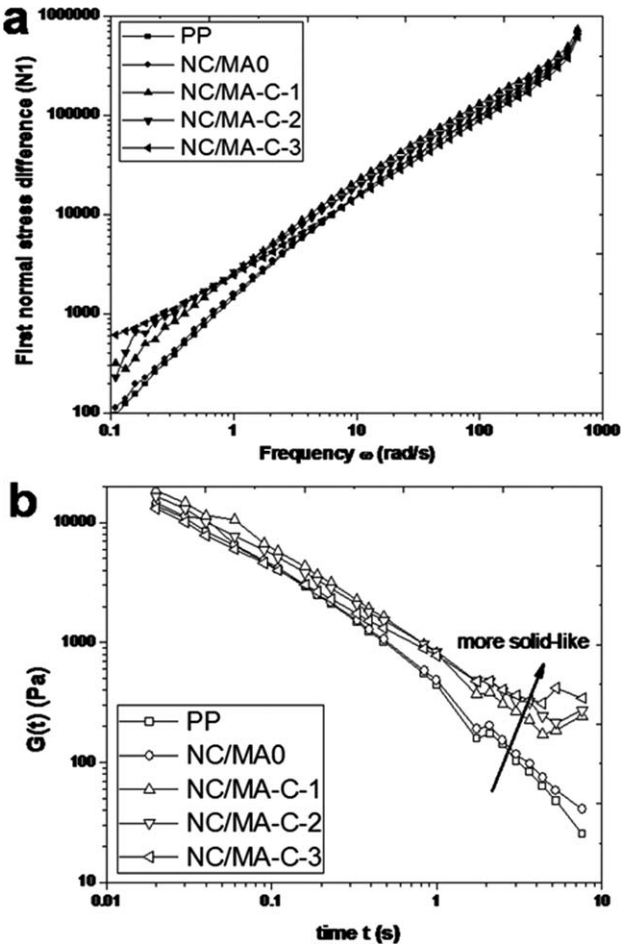

Figure 4. Stress relaxation behavior of neat PP and PP/clay nanocomposites: (a) first normal stress difference, and (b) stress relaxation modulus.

indicates exfoliation. The stress relaxation modulus of the PP/clay nanocomposites is shown in Table IV. In the beginning (0.02 s), the modulus of neat PP increased by 35% for the compatibilizer to clay ratio of 1 : 1 (4 phr clay loading), beyond which the stress relaxation modulus tends to decrease and in case of samples developed using 3 : 1 ratio of clay to compatibilizer the modulus even reaches below the value of neat PP. This increase in stress relaxation modulus is expected due to the presence of compatibilizer, and clay may not play any important role. But, at higher time interval, the polymer chains get more time to relax and the presence of exfoliated structure of clay developed with increase in compatibilizer content hinders the chain relaxation process. This is well reflected from the irregular increase in $G(t)$, where the modulus is increased by 158% in case of 1 : 1 compatibilizer to clay ratio whereas this increase is 220% and 252% for 2 : 1 and 3 : 1 ratio, respectively.

The inverse loss tangent and Cole–Cole plot can be taken as a measure to assess the dispersion of filler into polymer matrix. Figure 5(a) shows an inverse loss tangent plot as a function of loss modulus.[27,28] The linearity can be anticipated for PP without clay. Deviation from linearity is a measure of dispersed and percolated morphology. Addition of clay without compatibilizer shows a similar linear curve indicating poor dispersion of clay in absence of compatibilizer. With the addition of compatibilizer, shifting from linearity to non-linearity happens and deviation increases proportionally with increasing compatibilizer content. A deviation from arc-like shape in Cole–Cole plot is a measure of solid-like behavior. Figure 5(b) shows that increase in compatibilizer content improves dispersion which is reflected by the deviation of data for that of neat PP. In case of higher compatibilizer content (more than 2 : 1 compatibilizer to clay ratio), the curve seems to be almost linear. A sharp change in curvature (from NC/MA0 sample to NC/MA-C-1 sample) by addition of compatibilizer is also an indication of improved dispersion in the nanocomposites. Both 2 : 1 and 3 : 1 compatibilizer to clay ratios show a similar pattern up to η' ($= G''/\omega$) of about 2000 Pa s.

The steady torque is a qualitative indicator of stress that is imposed by the molten polymer and was assessed as a measure of clay exfoliation. It was found that the average steady torque value is reduced with increase in compatibilizer to clay ratio (Figure 6). This may be due to relatively lower melt viscosity and molecular weight of PP-*g*-MA as compared to those of PP. The higher torque value of PP/clay system without compatibilizer reveals an agglomerated morphology and is related to the higher energy required to break the clay structure. Addition of compatibilizer promotes dispersion and intercalation of polymer chains into clay gallery via rapid diffusion which is also reflected in the lower torque value.[29] The samples developed with compatibilizer to clay ratio of 2 : 1 and 3 : 1 show a slight variation in torque indicating 2 : 1 ratio to be the optimum.

TEM Analysis

The effect of compatibilizer content on the morphology of the nanocomposites was investigated with TEM at

Table IV. Stress Relaxation Modulus for Neat PP and PP/Clay Nanocomposites

	$G(t)$ (Pa)		
Compositions	At 0.02 s	At 7.6 s	$\Delta G(t) = [G(t)_{0.02} - G(t)_{7.6}]$ (Pa)
PP	13,776	25.4	13,750.6
NC/MA0	14,504	40.9	14,463.1
NC/MA-C-1	14,576	244.3	14,331.7
NC/MA-C-2	10,012	272.8	9,739.2
NC/MA-C-3	13,008	363.5	12,663.5

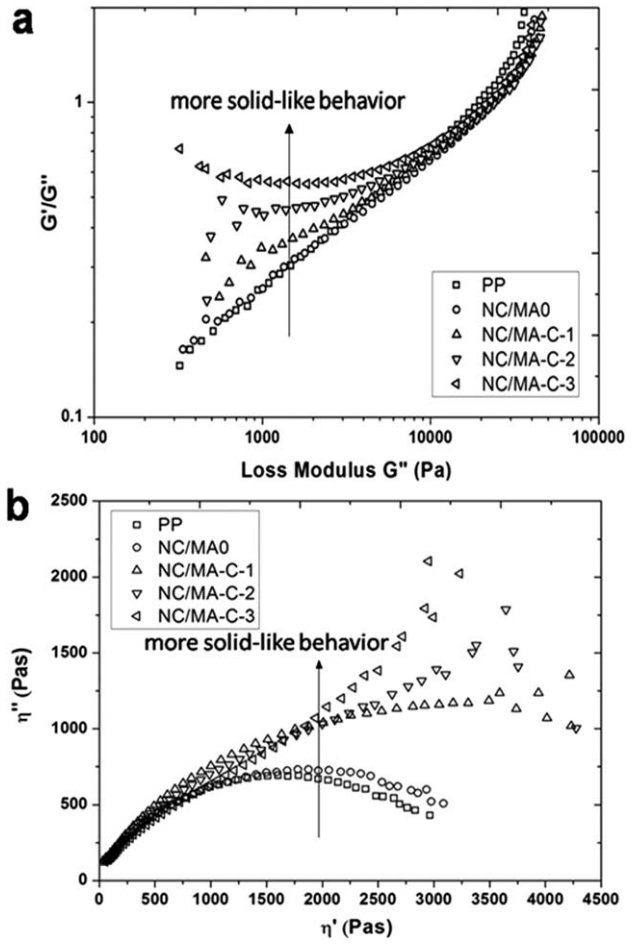

Figure 5. Rheological characterization of PP/clay nanocomposites: (a) inverse loss tangent and (b) Cole–Cole plot.

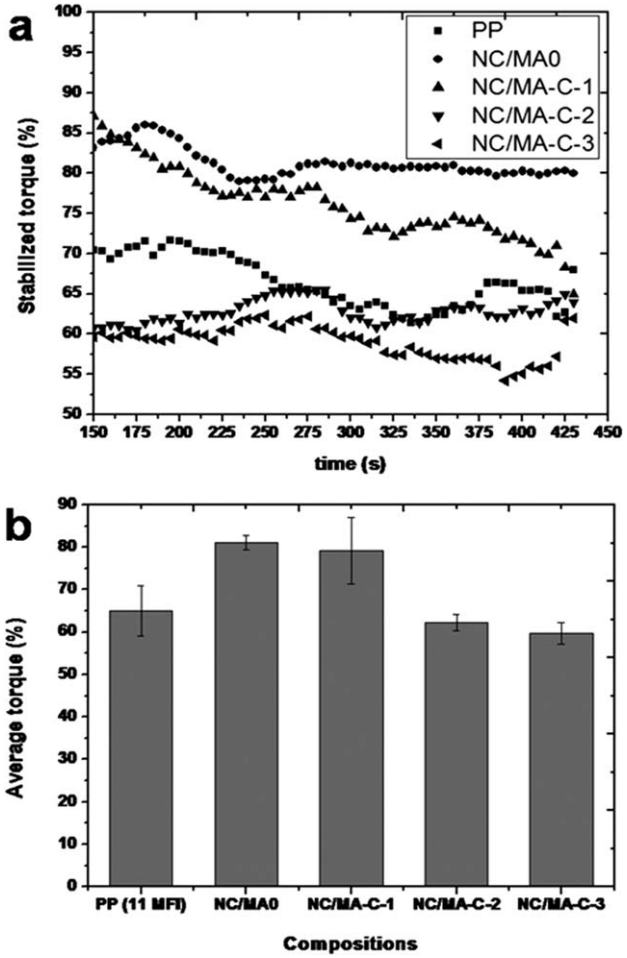

Figure 6. Effect of compatibilizer to clay ratio on (a) stabilized torque, and (b) average torque for unfilled PP and PP/clay nanocomposites during processing.

magnifications of 12–80 k×.[30] ImageJ software was used to measure the free-path distance, i.e., distance between the clay-platelets (ψ_{clay}), thickness of the tactoids, and intercalated stacks (d_{clay}).[31,32] Absence of PP-*g*-MA compatibilizer shows a tactoid morphology having a thickness range of 30 to 70 nm or more [Figure 7(a)]. With addition of compatibilizer at clay loading of 4 phr, the morphology shows presence of intercalated and intercalated/exfoliated in combination. The thickness of the lamellar stacks decreases to an average of 25 nm for a compatibilizer to clay ratio of 1 : 1 [Figure 7(b)]. Figure 7(c) and (d) shows similar type of morphology with a mixture of intercalated and exfoliated structure. The thickness of the intercalated structure lies at a minimum of 9 nm to maximum in the range of 35 nm. The length of the clay lamella (L_{clay}) is observed to be around 150 nm which demonstrates the peeling out of the individual clay platelets during intercalation. Better dispersion of the clay layers in presence of the compatibilizer to clay ratio of 2 : 1 and above is corroborated by higher free-path (ψ_{clay}) distance above 100 nm between the dispersed clay layers. But a higher compatibilizer to clay ratio is also responsible for inferior mechanical properties [Figure 9(b)] as the presence of compatibilizer (PP-*g*-MA) lowers the overall molecular weight.

Morphology from *Image Analysis*

A thorough study of morphology was performed using TEM images of PP/Clay nanocomposites at lower (12 k×) to higher (80 k×) magnifications. At least 8–10 images were considered to have a thorough idea of the overall morphology of each samples. The images at lower magnifications are more informative as it covers more sample area, so large number of TEM images of lower magnification was considered. Individual thickness of Cloisite 15A platelet and gallery spacing was taken from literature as 0.94 and 3.15 nm, respectively.[33] The images were converted to binary and then to threshold for better resolution and contrast. Calibration of the scale bar was performed to convert pixel unit into length and finally measurement of various parameters like particle area, thickness, length, aspect ratio, and particle density were done. Figure 8 shows a binary and outlined image of nanocomposite having a composition of 2 : 1 compatibilizer to clay ratio (processed at 300 rpm, NC/MA-C-2) at 12 k× magnification.

Frequency of mean free-path distance and various types of clay stacks is shown in Figure 9(a). The mean free-path distance is the average shortest distance of two adjacent clay particles. The

Applied Polymer SCIENCE

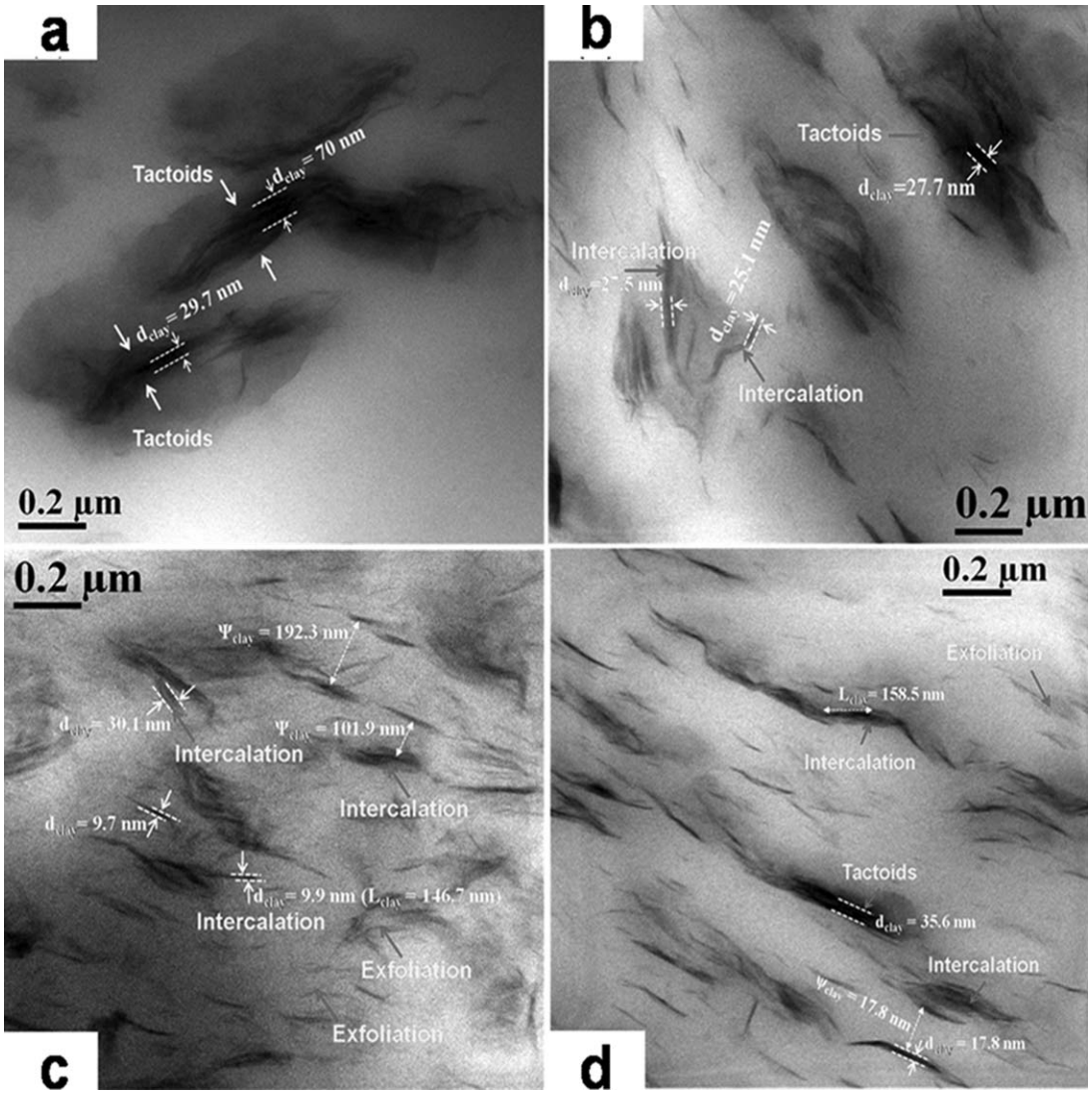

Figure 7. Transmission electron microscopic images of PP/clay nanocomposites having various compatibilizer to clay content: (a) without compatibilizer, (b) 1 : 1 ratio, (c) 2 : 1 ratio, and (d) 3 : 1 ratio (12 k× magnification).

mean free path spacing is larger (above 160 nm) for only PP/clay composition without compatibilizer (Table V). It signifies that, in absence of compatibilizer the clays are in tactoid/large agglomerated form and non-homogeneously distributed in different domains. Addition of compatibilizer improves dispersion which is reflected by a large occurrence of clay particles having lower free path spacing (below 120 nm). It means more number of particles are homogenously dispersed and are quite close to each other showing the presence of exfoliated morphology. It can also be seen that the composition having 2 : 1 compatibilizer to clay ratio shows more abundance of particle within this mean free path spacing (<60 nm), i.e., this composition seems to have better morphology. The intercalated/exfoliated morphology can be well demonstrated from the occurrence of various types of clay aggregates/tactoids shown in Figure 10(b). Thickness of the individual clay platelet is measured as 0.92 nm from image analysis and gallery spacing is taken as 3.15 nm. Based on this data, the tactoids having thickness in between 40–60 nm is designated as small tactoids with more than 10 platelets and those above 60 nm as aggregates. Among all the compositions, absence of compatibilizer shows more numbers of aggregates along with some 8–10 sheets tactoids. Addition of compatibilizer improves intercalation and exfoliation which is supported by large occurrence of individual clay platelets and 2–4 platelet stacks. Weight average length and aspect ratio of stacks, tactoid percentage and particle density are some important parameters to investigate the intercalated and/or exfoliated morphology of a nanocomposite. The weight average parameter can be expressed as,

$$P_w = \Sigma n_i P_i^2 / \Sigma n_i P_i \quad (5)$$

where n_i and P_i are the number and value of the ith parameter, respectively. Peeling out of clay platelets from the tactoids promotes clay dispersion and exfoliation. Figure 10(c) shows an increase in tactoid lengths with increase in compatibilizer content as a result of peel out of layers. The effect is

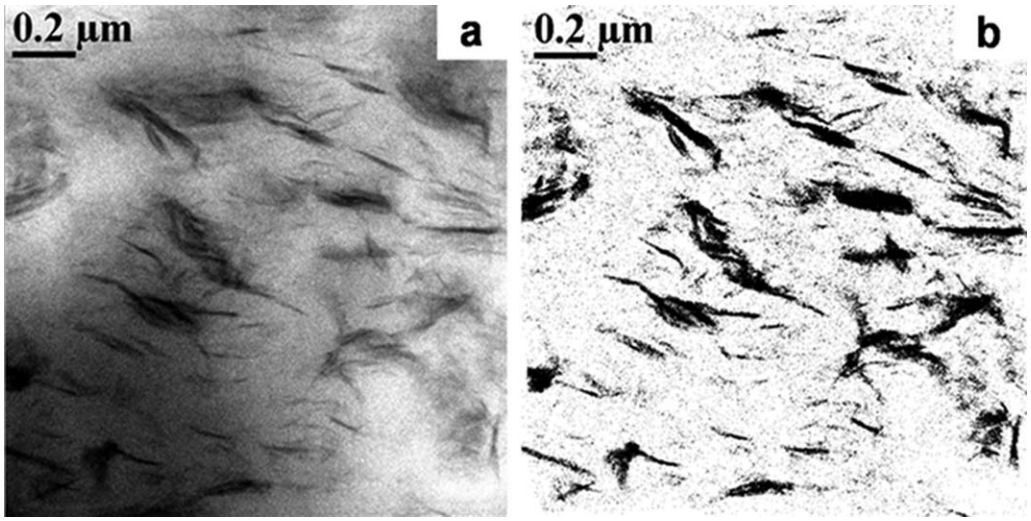

Figure 8. Image analysis of TEM micrographs for of PP/clay nanocomposites with 2 : 1 compatibilizer to clay ratio: (a) original image and (b) binary image (12 k× magnification).

more prominent in case of higher compatibilizer to clay ratio (3 : 1). Table V shows an increase in particle density and tactoids average aspect ratio with addition of compatibilizer. A reduction of tactoid area by ~29% was found in case of 3 : 1 ratio.

Dielectric and Mechanical Properties

Figure 10(a) shows the plot of dielectric constant (ε) of pure polypropylene and clay nanocomposites as a function of frequency (log f). The dielectric constants decrease with the increase in frequency and the change in dielectric constant value is more significant at lower frequency. The difference in relative permittivity (dielectric constant) at low frequency (0.1 MHz) and high frequency (10 MHz) is called the dielectric dispersion.[34,35] Higher is the value, better is the dispersion and exfoliation. In case of neat polypropylene, the dielectric dispersion factor is about 0.89 and on addition of clay only the factor does not change much. When compatibilizer is added, the factor suddenly rises to 1.36 and it is maximum (~1.52) for the composition having 2 : 1 compatibilizer to clay ratio. This fact supports for the better dispersion of organoclay in presence of PP-*g*-MA compatibilizer. Addition of organo-clay improves the

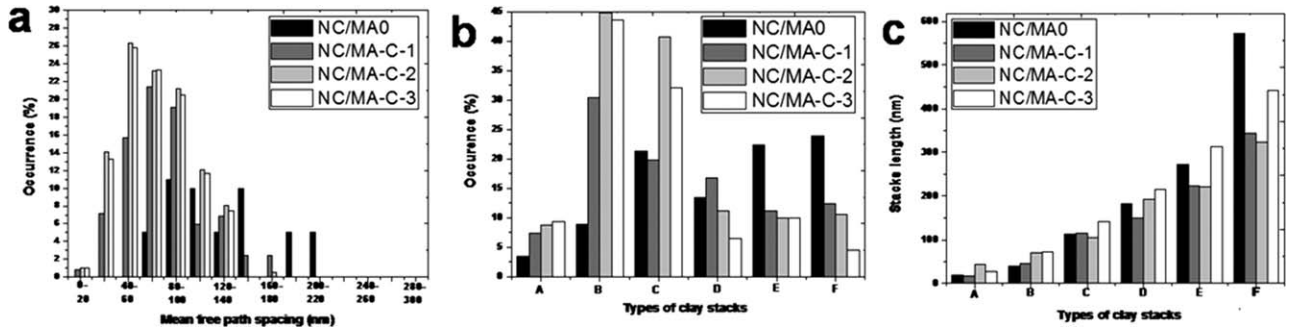

Figure 9. A comparative study of occurrence of (a) mean free path spacing of clay stacks, (b) different classes of clay stacks, and (c) weight-average length. [A: individual platelet (<4 nm thickness), B: 2–4 platelets (5–15 nm thickness), C: 5–7 platelets (15–30 nm thickness), D: 8–10 platelets (30–40 nm thickness), E: 40–60 nm thickness stacks, F: >60 nm thickness stacks].

Table V. Parameters Acquired from Image Analysis

Compositions	Total particles analyzed	Number of particles/unit image area	Tactoid (%)	Aspect ratio
NC/MA0	355	14	91.31	3.86
NC/MA-C-1	314	15	88.43	4.42
NC/MA-C-2	329	17	68.61	4.52
NC/MA-C-3	371	21	65.27	5.57

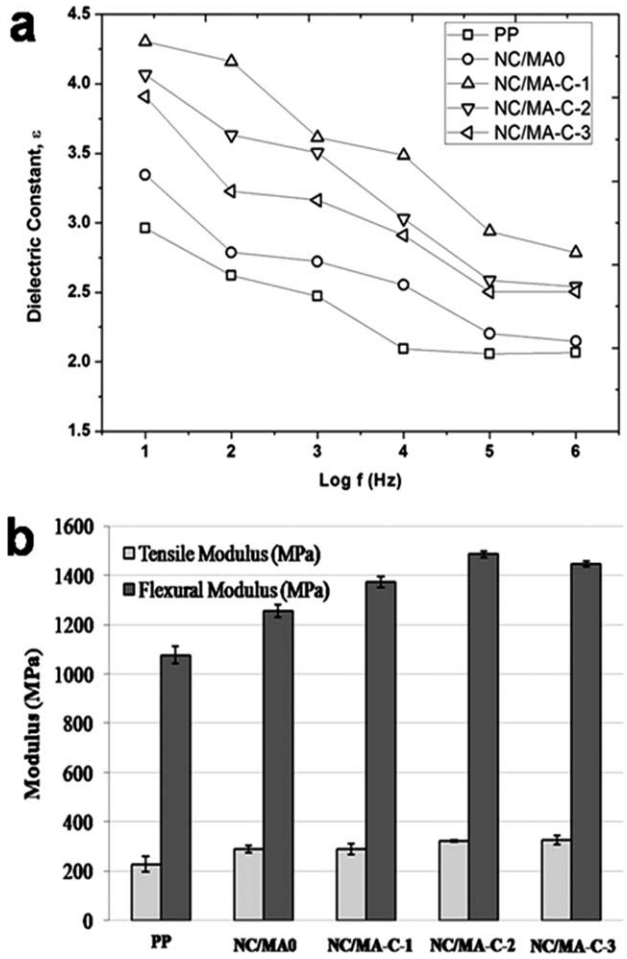

Figure 10. (a) Dielectric constant and (b) mechanical properties of neat PP and PP/clay nanocomposites.

dielectric constant value of PP (~2.96 at 10 Hz and 30°C) by 13% whereas compatibilizer addition increases the value by 45%. This rise is due to inclusion of polar PP-*g*-MA in PP matrix. Further increase in compatibilizer content is expected to increase the dielectric constant, but nanoscopic confinement plays a vital role in this case. Higher content of PP-*g*-MA compatibilizer promotes the exfoliation of the clay to form a network like percolated structure. Due to this percolated structure, more and more surface of clay sets exposed to hinder the orientation of the polar part in presence of applied electric field and as a result reduction in the dielectric constant value is seen.[36] The mechanical property of the nanocomposites as a function of compatibilizer content is shown in Figure 9(b). Both the tensile and flexural moduli improve by the addition of PP-*g*-MA[37] as compatibilizer addition facilitates contact between clay and the polymer by improving dispersion and exfoliation. Maximum increase in tensile modulus is found to be ~29% whereas for flexural modulus the increase is by 38%. At compatibilizer to clay content of 2 : 1 flexural modulus increases, and then it starts decreasing. The interaction parameter "*B*" derived from Turcsanyi model [eq. (6)] plays an important role to investigate the nanocomposites morphology.[38] More is the exfoliation, more is the interaction between clay platelets and matrix PP that results in a higher value of "*B*."

$$B = \left[\ln\left\{\sigma_y(\text{composite})/\sigma_y(\text{matrix})\right\} + \ln(1+2.5\varphi_f/1-\varphi_f)\right]/\varphi_f \quad (6)$$

where σ_y(matrix): yield strength of matrix, σ_y(composite): yield strength of composite, Φ_f: volume fraction of filler clay, *B*: interfacial interaction parameter between polymer and clay. Table VI shows an increase in yield strength and "*B*" value with increasing compatibilizer to clay ratio with helped in dispersion. But inclusion of stiffer clay reduced the elongation of the PP matrix at break.

CONCLUSIONS

The image analysis technique based on TEM micrographs was used to quantitatively characterize the dispersion and exfoliation of organo-clay in PP matrix. The effect of varying compatibilizer (PP-*g*-MA) to clay content on final morphology of nanocomposites has also been investigated. A wide range of parameters like average length, thickness, aspect ratio of the clay tactoids with their relative proportions was determined from the analysis. Decrease in tactoid percentage and increase in aspect ratio with increasing compatibilizer content indicates better dispersion and exfoliation. Since TEM-analysis is not reliable when used alone, supportive tools like melt rheology, dielectric, and mechanical testing were also performed. Enhancements of storage and relaxation modulus, complex viscosity at low frequency region as well as change in cross-over frequencies and Cole–Cole plots for sample with compatibilizer indicate improved morphology.

Study of dielectric and mechanical properties provide important information about the nanocomposite microstructure. It was found that with clay dispersion and exfoliation, the "dielectric dispersion" and the mechanical properties also get enhanced. But the improvement was maximum at 2 : 1 compatibilizer to

Table VI. Mechanical Properties of PP and PP/Clay Nanocomposites

Compositions	Yield strength, σ_y (MPa)	Elongation (%) at break	Volume fraction of clay, Φ_f	Interaction parameter, *B*
PP	27.50	26.35	0	0
NC/MA0	27.39	23.39	0.0215	3.238
NC/MA-C-1	28.21	34.04	0.0206	4.684
NC/MA-C-2	29.63	28.62	0.0199	7.203
NC/MA-C-3	29.90	25.16	0.0192	7.810

clay ratio. Beyond this ratio the nanocomposites experienced inferior material properties and it may be solely due to cut-down of matrix molecular weight due to presence of high compatibilizer content. The dielectric constant value was found to fall with increased compatibilizer content. It happens due to confinement of polymer chains by the percolated network structure of clay commonly known as "nanoscopic confinement."

REFERENCES

1. Giannelis, E. P.; Krishnamoorti, R.; Manias, E. *Adv. Polym. Sci.* **1999**, *138*, 107.
2. Alexandre, M.; Dubois, P. *Mater. Sci. Eng.* **2000**, *28*, 1.
3. Ray, S. S.; Okamoto, M. *Prog. Polym. Sci.* **2003**, *28*, 1539.
4. Chen, B.; Evans, J. R. G.; Greenwell, H. C.; Boulet, P.; Coveney, P. V.; Bowden, A. A.; Whiting, A. *Chem. Soc. Rev.* **2008**, *37*, 568.
5. Paul, D. R.; Robeson, L. M. *Polymer* **2008**, *49*, 3187.
6. Kurokawa, Y.; Yasuda, Y. H.; Kashiwagi, M.; Oya, A. *J. Mater. Sci. Lett.* **1997**, *16*, 1670.
7. Reichert, P.; Nitz, H.; Klinke, S.; Brandsch, R.; Thomann, R.; Mulhaupt, R. *Macromol. Mater. Eng.* **2000**, *275*, 8.
8. Kawasumi, M.; Hasegawa, N.; Kato, M.; Usuki, A.; Okada, A. *Macromolecules* **1997**, *30*, 6333.
9. Pinnavaia, T. J.; Beall, G. W. Polymer–Clay Nanocomposites; Wiley : New York, **2000**.
10. Krishnamoorti, R.; Ren, J.; Silva, A. S. *J. Chem. Phys.* **2001**, *114*, 4968.
11. Galgali, G.; Ramesh, C.; Lele, A. *Macromolecules* **2001**, *34*, 852.
12. Wagener, R.; Reisinger, T. J. G. *Polymer* **2003**, *44*, 7513.
13. Vermogen, A.; Varlot, K. M.; Seguela, R.; Rumeau, J. D.; Boucard, S.; Prele, P. *Macromolecules* **2005**, *38*, 9661.
14. Anastasiadi, H.; Karataso, K.; Vlachos, G.; Manias, E.; Giannelis, E. P. *Phys. Rev. Lett.* **2000**, *84*, 915.
15. Smyth, C. P. Dielectric Behavior and Structure; McGraw Hill: New York, **1955**.
16. Banerjee, S.; Joshi, M.; Ghosh, A. K. *J. Appl. Polym. Sci.* **2012**, *123*, 2042.
17. Zujo, V. P.; Gupta, R. K.; Bhattacharya, S. N. *Rheol. Acta* **2004**, *43*, 99.
18. Ren, J.; Silva, A. S.; Krishnamoorti, R. *Macromolecules* **2000**, *33*, 3739.
19. Graebling, D.; Muller, R.; Palierne, J. F. *Macromolecules* **1993**, *26*, 320.
20. Alexandre, M.; Dubois, P. *Mater. Sci. Eng. R* **2000**, *28*, 1.
21. Nam, P. H.; Kaneko, M.; Ninomiya, N.; Fujimori, A.; Masuko, T. *Polym. Int.* **2006**, *55*, 916.
22. Li, J.; Zhou, C. X.; Wang, G.; Zhao, D. *J. Appl. Polym. Sci.* **2003**, *89*, 318.
23. Solomon, M. J.; Almusallam, A. S.; Seefeldt, K. F.; Varadan, P. *Macromolecules* **2001**, *34*, 1864.
24. Wu, D. F.; Zhou, C. X.; Xie, F.; Mao, D. L.; Zhang, B. *Eur. Polym. J.* **2005**, *41*, 2199.
25. Schwarzl, F. R. *Rheol. Acta* **1975**, *14*, 581.
26. Lim, S. K.; Hong, E. P.; Song, Y. H.; Park, B. J.; Choi, H. J.; Chin, I. *J. Polym. Eng. Sci.* **2010**, *50*, 504.
27. Sepehr, M.; Utracki, L. A.; Zheng, X. X.; Wilkie, C. A. *Polymer* **2005**, *46*, 11569.
28. Utracki, L. A.; Jorgensen, L. *Rheol. Acta* **2002**, *41*, 394.
29. Hasegawa, N.; Kawasumi, M.; Kato, M.; Usuki, A.; Okada, A. *J. Appl. Polym. Sci.* **1998**, *67*, 87.
30. Dumont, M. J.; Valencia, A. R.; Emond, J. P.; Bousmina, M. *J. Appl. Polym. Sci.* **2007**, *103*, 618.
31. Abramoff, M. D.; Magelhaes, P. J.; Ram, S. *J. Biophoton. Int.* **2004**, *11*, 36.
32. Luo, Z. P.; Koo, J. H. *Polymer* **2008**, *49*, 1841.
33. Chavarria, F.; Paul, D. R. *Polymer* **2004**, *45*, 8501.
34. Smith, T. W.; Abkowitz, M. A.; Conway, G. C.; Luca, D. J. S.; Wnek, G. E. *Macromolecules* **1996**, *29*, 5046.
35. Wang, H. W.; Chang, K. C.; Chu, H. C.; Liou, S. J.; Yeh, J. M. *J. Appl. Polym. Sci.* **2004**, *92*, 2402.
36. Tanaka, T. *IEEE Trans. Dielect. Electric. Insul.* **2005**, *12*, 914.
37. Tarapow, J. A.; Bernal, C. R.; Alvarez, V. A. *J. Appl. Polym. Sci.* **2009**, *111*, 768.
38. Turcsanyi, B.; Pukanszky, B.; Tudos, F. J. *Mater. Sci. Lett.* **1988**, *7*, 160.